JACS
JOURNAL OF THE AMERICAN CHEMICAL SOCIETY

Article

pubs.acs.org/JACS

Switching the Spin State of Diphenylcarbene via Halogen Bonding

Stefan Henkel,[†] Paolo Costa,[†] Linda Klute,[†] Pandian Sokkar,[‡] Miguel Fernandez-Oliva,[‡] Walter Thiel,[‡] Elsa Sanchez-Garcia,*[,‡] and Wolfram Sander*[,†]

[†]Lehrstuhl für Organische Chemie II, Ruhr-Universität Bochum, 44801 Bochum, Germany

[‡]Max-Planck-Institut für Kohlenforschung, 45470 Mülheim an der Ruhr, Germany

Supporting Information

ABSTRACT: The interactions between diphenylcarbene DPC and the halogen bond donors CF_3I and CF_3Br were investigated using matrix isolation spectroscopy (IR, UV−vis, and EPR) in combination with QM and QM/MM calculations. Both halogen bond donors CF_3X form very strong complexes with the singlet state of DPC, but only weakly interact with triplet DPC. This results in a switching of the spin state of DPC, the singlet complexes becoming more stable than the triplet complexes. CF_3I forms a second complex (type II) with DPC that is thermodynamically slightly more stable. Calculations predict that in this second complex the DPC···I distance is shorter than the F_3C···I distance, whereas in the first (type I) complex the DPC···I distance is, as expected, longer. CF_3Br only forms the type I complex. Upon irradiation I or Br, respectively, are transferred to the DPC carbene center and radical pairs are formed. Finally, on annealing, the formal C−X insertion product of DPC is observed. Thus, halogen bonding is a powerful new principle to control the spin state of reactive carbenes.

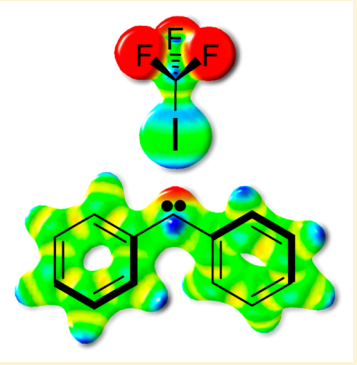

INTRODUCTION

Halogen bonding has long been recognized as an important principle for stabilizing intermolecular complexes DX···A, where DX is the halogen bond donor with X = Cl, Br, or I, and A is a Lewis base as halogen bond acceptor bearing a lone electron pair that interacts with the X atom of the donor.[1−3] The stability of halogen bonds DX···A can be similar to that of the much better studied hydrogen bonds DH···A, and therefore halogen bonding can be the dominant intermolecular interaction in weakly bound aggregates. In a computational study comparing halogen with hydrogen bonds, Wolters and Bickelhaupt concluded that both have large covalent components stemming from HOMO−LUMO interactions.[1] In many of the examples studied, the halogen bonds are characterized by weaker electrostatic attractions and stronger stabilizing HOMO−LUMO interactions than the hydrogen bonds. In line with this is the observation that the directionality of halogen bonds is even more pronounced than that of hydrogen bonds, strongly preferring linear orientations of DX···A.[4] Halogen atoms increase the hydrophobicity of organic molecules, and therefore halogen bonding has been considered as a hydrophobic equivalent of the hydrophilic hydrogen bonding.[5] The large covalent contribution to halogen bonds renders them more resistant to increasing solvent polarity, as recently has been outlined by Hunter et al.[6]

Because of these properties, which complement the traditional hydrogen bonds, halogen bonds play important roles in molecular aggregation, in particular in supramolecular assembly and in crystallization processes.[5−8] In contrast, much less is known about the influence of halogen bonding on reactive intermediates and transition states, and therefore on the kinetics of chemical reactions. Huber et al. demonstrated that carbon−heteroatom bonds can be activated by multidentate halogen bonding,[9] and on this basis developed efficient organocatalysts.[10] Many solvents and reagents are halogenated, and in these cases the reactivity and selectivity of reactions might be influenced by halogen bonds stabilizing short-lived reaction intermediates. Here, we describe how halogen bonds entirely can change the properties of a reactive carbene intermediate by switching its ground state from triplet to singlet.

Since singlet carbenes R_2C: are strong Lewis bases, it is expected that these species are stabilized by halogen bonds. Therefore, carbene chemistry should be strongly affected by solvents and reagents X-R′ that are able to act as halogen bond donors in carbene complexes R_2C···X-R′. An early example for a halogen bond between a stable N-heterocyclic carbene (NHC) as halogen bond acceptor and pentafluoroiodobenzene as donor was published by Arduengo et al. in 1991.[11] The X-ray structure analysis of this complex **1** reveals a nearly linear C−I−C bond (178.9°) and a C−I bond length of 2.75 Å between the iodine atom and the carbene center. The bonding was described as "reverse ylide" with a positively charged carbene center and a negatively charged iodine atom. A similar complex **2**, in which an iodine atom interacts with two stable nucleophilic carbenes, was described three years later.[12]

Other direct experimental evidence for halogen-bonded carbenes has not been reported. A recent theoretical study investigates the interactions between the nucleophilic carbene **3**

Received: December 5, 2015

DOI: 10.1021/jacs.5b12726
J. Am. Chem. Soc. XXXX, XXX, XXX−XXX

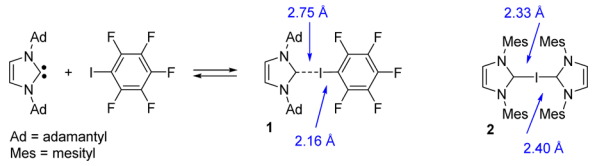

as a model acceptor with a variety of halogen bond donors.[13] Interestingly, two types of complexes were predicted, depending on the bond dissociation energy (BDE) of the D−X bond. If the BDE is large, as in most DX molecules containing C−X or H−X bonds, the expected classical halogen-bonded complexes with long distances between the carbene center and the halogen atom are predicted. The binding energies of these type I complexes are calculated between 1.5 (CH_3−Cl as donor) and 13 kcal/mol (NC-Br as donor). On the other hand, if the BDE is small, as in the dihalogen or interhalogen molecules, a different structure with much larger binding energies (e.g., 48 kcal/mol for F−Br as donor) and short distances between the carbene center and the halogen atom is found. These type II complexes are described as ion-pair complexes between the D^- and X-3^+ charged fragments.[13] The transfer of an X^+ ion from the halogen bond donor to the acceptor therefore resembles the proton transfer in hydrogen bond complexes.

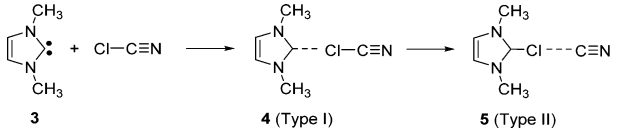

An interesting case is the interaction of NHC **3** with ClCN, where both the type I and the type II complex were predicted to exist as minimum structures: the conventional type I complex **4** with a binding energy of 7.7 kcal/mol and the unconventional type II complex **5** with a negative binding energy of −9.9 kcal/mol (with respect to the monomers **3** and ClCN). Complex **5** lies in a very shallow minimum and is only metastable.

The only experimentally characterized halogen-bonded carbene complexes are the two NHC complexes **1** and **2**.[11,12] In addition, a few theoretical studies on carbenes as halogen bond acceptors were published.[13,14] Halogen-bonded complexes of reactive carbenes are entirely unknown, and even hydrogen-bonded complexes of these species were rarely studied.

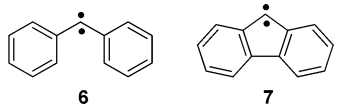

We recently demonstrated that hydrogen bonds strongly influence the reactivity of diphenylcarbene (DPC) **6**[15,16] and fluorenylidene **7**.[17] DPC **6** is a ground state triplet carbene with a singlet triplet gap ΔG_{ST} of −4.75 kcal/mol in isooctane and of −3.36 kcal/mol in acetonitrile.[18] Since singlet S-**6** is more polar than triplet T-**6**, the singlet state is better stabilized in solvents of higher polarity, and consequently, ΔG_{ST} is getting smaller with increasing solvent polarity. However, even in methanol glass at cryogenic temperatures, T-**6** remains more stable than S-**6**, which is easily demonstrated by EPR spectroscopy.

The reaction of carbene **6** with methanol has been widely investigated[19−21] as a model reaction to demonstrate the spin-specifity of carbene reactions: T-**6** is expected to undergo radical-like C−H abstractions to form a radical pair, whereas S-**6** inserts into the O−H bond either concerted or stepwise via ionic intermediates such as ylides or ion pairs. In solid methanol above 70 K, carbene **6** reacts to give the O−H insertion product **8**,[22] whereas at temperatures below 50 K it is unreactive even on a time scale of days. In striking contrast, carbene **6** rapidly reacts with CH_3OH in argon matrices doped with 1% of CH_3OH at temperatures as low as 25 K.[15] At temperatures between 25 and 30 K solid argon is getting soft, and small molecules such as CH_3OH are allowed to diffuse and undergo bimolecular reactions with **6**. At temperatures below 15 K argon is very rigid, and thus diffusion effectively inhibited. These observations demonstrate that (i) single molecules of CH_3OH are highly reactive toward **6** at 25 K, whereas bulk methanol at the same temperature does not react, and (ii) carbene **6** exclusively reacts via its (excited) singlet state S-**6** even at cryogenic temperatures.

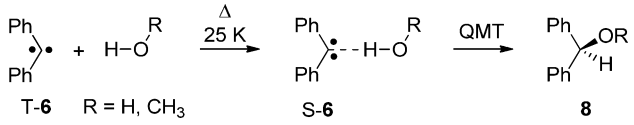

This reactivity pattern is not limited to carbene **6** and to CH_3OH: in 1% H_2O-doped argon matrices the corresponding metastable water complex S-**6**···HOH is formed,[16] and fluorenylidene **7** reacts with H_2O to the analogous complex S-**7**···HOH.[17] The switching of the ground states of carbenes **6** and **7** from triplet to singlet results from the strong hydrogen bonds with methanol or water that stabilize the singlet states, whereas the triplet states form only weak van der Waals interactions. If the difference in complexation energy between the singlet and the triplet states of a carbene with triplet ground state is larger than the S-T energy gap, the ground state is expected to be switched to singlet by hydrogen bonding.

Halogen bonds should be able to stabilize the singlet state S-**6** in a similar way as hydrogen bonds, and we therefore investigated the reaction of carbene **6** with CF_3I and CF_3Br as halogen bond donors. These donors were selected since they have been shown to form strong halogen bonds with various Lewis bases,[23−26] and in addition are small enough to diffuse in solid argon during annealing. Thus, warming a CF_3I-doped argon matrix from 8 to 25 K results in the formation of van der Waals dimers.[27] This ability to diffuse in solid argon is prerequisite for inducing bimolecular chemistry under the conditions of matrix isolation.

RESULTS AND DISCUSSION

DPC−CF_3I Reaction: IR Spectra. Triplet diphenylcarbene T-**6** was generated by 530 nm photolysis of diphenyldiazomethane **9**, matrix-isolated in argon doped with 1% of CF_3I at 3 K. The carbene was identified by IR, EPR and UV−vis spectroscopy.[15,16,28] Subsequent annealing at 25 K allows CF_3I to diffuse in the matrix, and after 10 min at this temperature the IR bands of T-**6** and CF_3I decrease in intensity and new signals are formed (Figure 1b). The weakly bound dimers of CF_3I show only small shifts of the IR bands compared to the monomer[29] and are easily identified. Other newly formed bands can be assigned to a complex between singlet carbene S-**6** and CF_3I by comparison with the spectra of the methanol or the water complex of S-**6**.[15,16] Highly characteristic in the complexes S-**6**···HOH and S-**6**···$HOCH_3$ is the asymmetrical CCC stretching vibration across the carbene center at 1328

DOI: 10.1021/jacs.5b12726
J. Am. Chem. Soc. XXXX, XXX, XXX−XXX

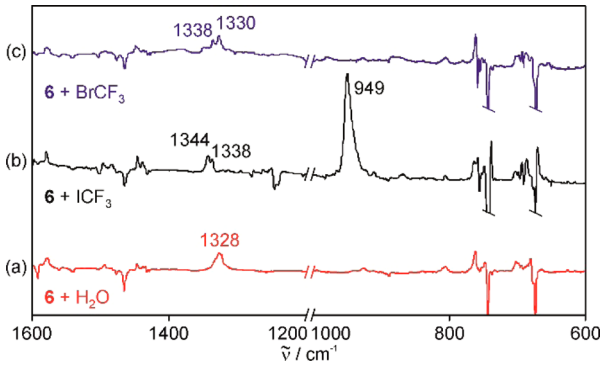

Figure 1. IR difference spectra showing the reaction of diphenylcarbene **6** with (a) H_2O (red, see ref 16), (b) CF_3I (black), and (c) CF_3Br (blue). The reactions are induced by warming argon matrices containing **6** and H_2O, CF_3I, or CF_3Br, respectively, from 3 to 25 K. The region between 1000 and 1200 cm^{-1} containing strong CF_3X vibrations is omitted for clarity (see SI for the full spectrum).

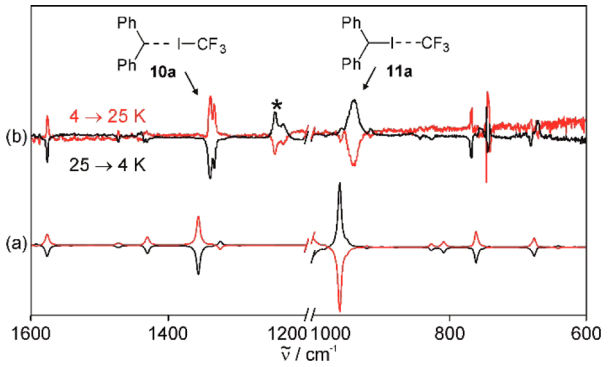

Figure 2. IR difference spectra showing the reversible thermal interconversion between complexes **10a** and **11a**. (a) Difference spectra calculated at the B97-D3/def2-TZVP level of theory; black: **10a** converted to **11a**, red: **11a** converted to **10a**. (b) Experimental difference spectra; black: cooling the matrix from 25 to 4 K, red: warming the matrix from 4 to 25 K. The spectra were recorded after multiple cycles of annealing to reduce matrix site effects. Bands of the CF_3 radical are labeled with an asterisk. The region between 1000 and 1200 cm^{-1} containing strong CF_3X vibrations is omitted for clarity (see SI for the full spectrum).

cm^{-1} (Figure 1a). In the S-**6**···ICF_3 complex **10a** this vibration is slightly blue-shifted and split into two components at 1338 and 1344 cm^{-1}.

The IR spectrum of the S-**6**···ICF_3 complex **10a** is in good agreement with DFT calculations at the B97-D3/def2-TZVP level of theory. The triplet carbene complex T-**6**···ICF_3 is predicted to be higher in energy by 3.7 kcal/mol, and the spectrum calculated for the triplet complex does not match the experimental spectrum. These results clearly indicate that the interaction between triplet carbene T-**6** and CF_3I results in a strong stabilization of S-**6** via halogen bonding.

The IR difference spectrum (Figure 1b) indicates the formation of several species in addition to **10a**. The most prominent additional band is a very intense signal centered at 949 cm^{-1}. This signal is assigned to an unconventional type II halogen-bonded complex **11a** which is formally described as a halogen-bonded ion pair between CF_3^- and the diphenyl-(iodomethyl)cation.

CF_3^- was previously characterized by matrix isolation spectroscopy.[30] An IR band at 778 cm^{-1} was assigned to the degenerate, E symmetrical CF and FCF stretching vibration, and a band at 1050 cm^{-1} to the A_1 symmetrical CF_3 stretching vibration. In complex **11a**, the interaction between the two fragments results in a lowering of the symmetry and lifting of the degeneracy of the E vibration leading to two intense, strongly blue-shifted vibrations at 1139 and 1149 cm^{-1} (see below). The A_1 symmetrical CF stretching vibration is red-shifted to 949 cm^{-1}. A comparison of these characteristic vibrations of the CF_3 fragment in **11a** with that of CF_3^- and CF_3I reveals a much closer similarity to CF_3I than to CF_3^-, indicating that the CF_3 fragment in **11a** does not carry a large negative charge as in the anion.

Interestingly, the intensity ratio of the IR bands of complexes **10a** and **11a** depends on the temperature when cycling the temperature of the matrix between 4 and 25 K. At 4 K the IR bands of **11a** increase in intensity while those of **10a** decrease in intensity, whereas at 25 K the signals of **10a** increase and those of **11a** decrease (Figure 2). The thermal interconversion of the two complexes indicates that the equilibrium between these complexes is rapidly established even at cryogenic temperatures, and that the activation barrier for this process is essentially zero. Since the yield of type II complex **11a** is higher at lower temperatures, we conclude that **11a** is thermodynamically more stable than the 'classical' halogen-bonded type I complex **10a**.

The IR spectra taken during the thermal cycling between 4 and 25 K show that the CF_3 radical[29] with IR absorptions at 1242 and 1249 cm^{-1} is also formed (Figure 2). These bands are formed at temperatures below 10 K and disappear upon annealing of the matrix at 25 K. When the matrix is kept at 4 K inside the IR spectrometer, the signals of both complexes **10a** and **11a** decrease, accompanied by an increase of the bands of CF_3. This conversion can be suppressed by usage of an interference filter, blocking light above 2000 cm^{-1}, which indicates that complexes **10a** and **11a** are very photolabile, and irradiation by the glow bar of the IR spectrometer results in rapid photolysis.

The IR absorptions of CF_3 at 1242 and 1249 cm^{-1} agree well with those obtained after UV photolysis of matrix isolated CF_3I (1247 and 1252 cm^{-1}).[29] The band at 1252 cm^{-1} was assigned to the "free" CF_3 radical, the band at 1247 cm^{-1} to the CF_3···I radical pair.[29] Accordingly, the two signals observed in our experiments are assigned to free CF_3 and to the Ph_2C—I···CF_3 radical pair **12a**. A good agreement between the experimental and theoretical spectrum is found in both cases (see SI). On annealing the matrix at 25 K the radical pair **12a** is expected to recombine, which explains the decrease of intensity of **12a** during warming the matrix.

The frequency of the E symmetrical IR vibration of CF_3 strongly depends on the charge and shifts from 1662 cm^{-1} in CF_3^+ to 1284 in the CF_3 radical to 778 cm^{-1} in CF_3^-. In CF_3I this vibration is found at 1175 cm^{-1} which suggests a small negative partial charge (Figure 3). Complex **10a** exhibits the corresponding vibration at 1103 cm^{-1}, and **11a** at 1139 and 1149 cm^{-1}, quite close to CF_3I. This is in line with the calculations and suggests that there is no strongly negative charged CF_3 fragment in these complexes.

After the initial annealing of matrices containing T-**6** and CF_3I, the formal insertion product of carbene **6** into the CI bond of CF_3I, iodo-2,2,2-trifluoro diphenylethane **13a**, is only a minor byproduct. The formation of the metastable species **10a**, **11a**, and **12a** demonstrates that the matrix effectively inhibits rearrangement to **13a**, despite calculations (B97-D3/def2-

DOI: 10.1021/jacs.5b12726
J. Am. Chem. Soc. XXXX, XXX, XXX−XXX

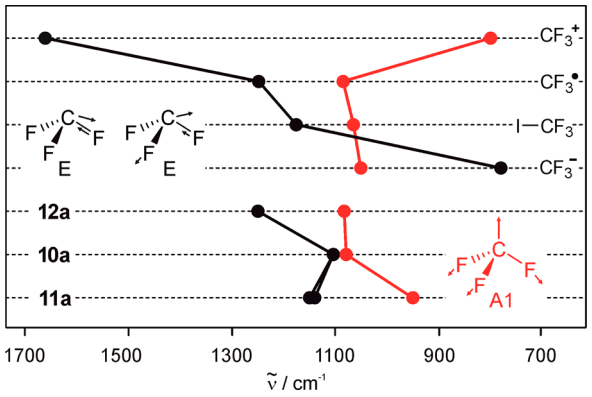

Figure 3. Characteristic vibrations of the CF_3 fragment. The experimental frequencies of the degenerate, E symmetrical CF and FCF stretching vibrations (black) and of the A_1 symmetrical CF_3 stretching vibration (red) strongly depend on the charge of the CF_3 group: cation CF_3^+,[30] radical CF_3,[29] neutral CF_3I, and anion CF_3^-[30] (upper four traces) are compared to **12a**, **10a** and **11a** (three lower traces).

TZVP) predict the formation of **13a** from T-**6** and CF_3I to be strongly exothermic by 67 kcal/mol. However, prolonged irradiation (450 nm) results in a decrease of the signals of carbene **6**, remaining **9**, complexes **10a** and **11a**, and radical pair **12a** and formation of the final product **13a** (Scheme 1). The observed IR bands fit reasonably well to the calculated spectrum of **13a**.

Scheme 1. Reaction of Diphenylcarbene 6 with ICF_3

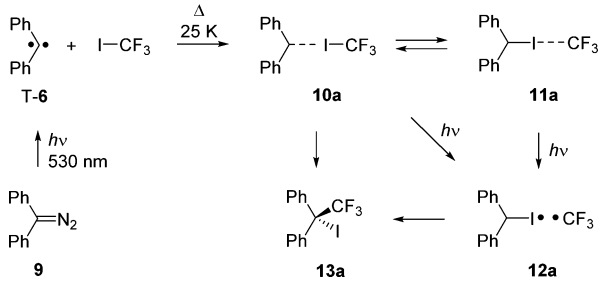

DPC–CF_3I Reaction: UV–Vis Spectra. The formation of **10a** from T-**6** and CF_3I could also be monitored by UV–vis spectroscopy (Figure 4). Upon annealing of an argon matrix containing both carbene T-**6** and CF_3I, the characteristic weak visible absorption of T-**6** at 458 nm[31] decreases, and simultaneously a UV absorption at 372 nm and a very broad absorption in the visible region centered around 930 nm appear (Figure 4). The singlet carbene complexes S-**6**···HOR (R = H, CH_3) exhibit a UV absorption at 360 nm assigned to singlet carbene S-**6**,[15,16] and therefore we assign the band at 372 nm to **10a**.

Multistate CASSCF(12,12) calculations predict a near IR transition for type 1 complex **10a** at 944 nm and for the type II complex **11a** at 784 nm (see Supporting Information for the computational details), both corresponding to HOMO–LUMO type transitions. On this basis we assign the band at 930 nm to type I complex **10a**. Upon photolysis of the matrix with red light (650 nm) the bands assigned to **10a** decrease in intensity, in accordance with the observation in the IR experiments.

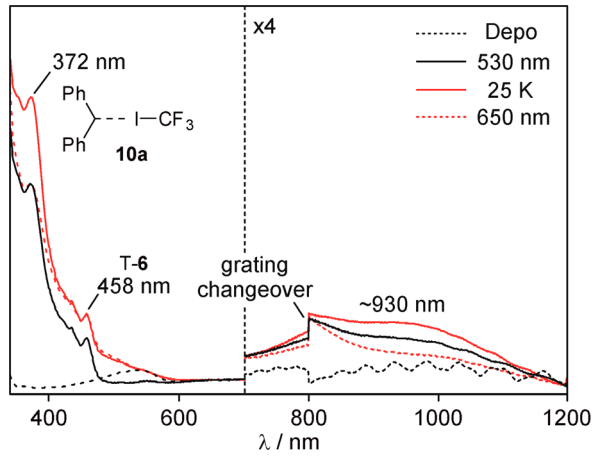

Figure 4. UV–vis spectra showing the reaction of T-**6** with CF_3I. Dashed black line: Spectrum of diphenyldiazomethane **9** in argon doped with 1% of CF_3I at 10 K. Solid black line: Spectrum obtained after irradiation of the matrix with 530 nm light. Solid red line: Spectrum obtained after subsequent annealing of the matrix to 25 K for 10 min. Dashed red line: Spectrum after irradiation of the annealed matrix with 650 nm light. The cusp at 800 nm is due a grating change of the UV–vis spectrometer.

DPC–CF_3I Reaction: EPR Spectra. Photolysis of diazo precursor **9** in 1% CF_3I-doped Ar at 5 K produces the characteristic signals of T-**6** and a number of signals around 3400 G typical of radicals (Figure 5). The CF_3 radical is

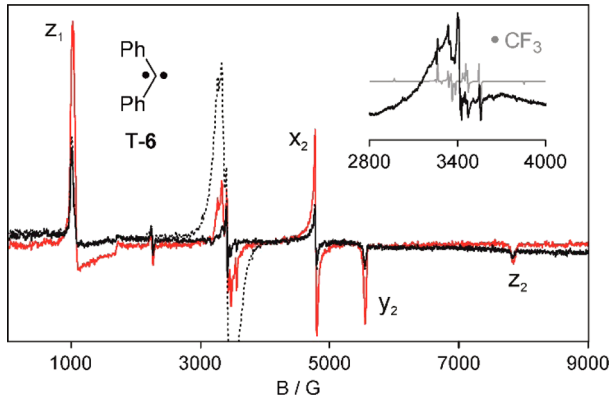

Figure 5. EPR spectra showing the reaction of triplet diphenylcarbene **6** with CF_3I. Red line: Spectrum of **6** in argon doped with 1% of CF_3I at 5 K. Solid black line: Spectrum of the same matrix after annealing to 25 K for 10 min. Dashed black line: Spectrum obtained after 650 nm irradiation. Inset shows the radical region together with a simulated spectrum of CF_3 radicals (see SI for details).

identified by its anisotropic hyperfine coupling pattern that was previously reported in literature.[32] Warming of the matrix from 5 to 25 K reduces the intensity of T-**6**, as expected if the EPR quiet singlet complexes **10a** and **11a** are formed. At the same time, the radical signals disappear, which is attributed to recombination as a result of the higher mobility of the radicals at higher temperatures. Subsequent irradiation of the matrix at 5 K with 650 nm light does not affect the signals of the triplet carbene, but results in the formation of an intense radical signal, consistent with the conversion of **10a** and **11a** to radical pair **12a** as observed in the IR experiments. The broad feature underlying the CF_3 signals is tentatively assigned to the Ph_2CI radical.

DOI: 10.1021/jacs.5b12726
J. Am. Chem. Soc. XXXX, XXX, XXX–XXX

DPC−CF_3Br Reaction. In an effort to explore the influence of the halogen atom on the halogen bond to carbene **6**, we also investigated the reaction with CF_3Br. If a matrix containing T-**6** and 0.5% of CF_3Br is annealed at 25 K, the resulting IR difference spectrum reveals the formation of S-**6**···$BrCF_3$ complex **10b** with a very similar IR spectrum as **10a** (Figure 2c, Scheme 2).

Scheme 2. Reaction of Diphenylcarbene 6 with $BrCF_3$

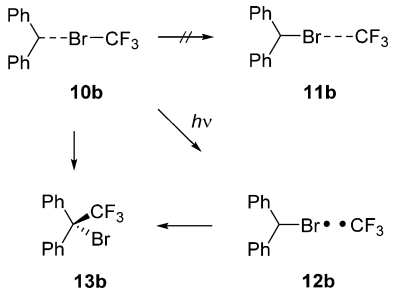

In **10b** the characteristic CCC stretching vibration of S-**6** is split into two components at 1330 and 1338 cm^{-1}, slightly red-shifted compared to **10a**. Interestingly, with CF_3Br a type II complex **11b** is not observed, as can be seen by the absence of an intense vibration around 949 cm^{-1}. Photolysis of **10b** with 650 nm light leads to formation of CF_3 radicals and the Ph_2C−Br···CF_3 radical pair **12b**, in analogy to the photochemistry of **10a**. The radical pair **12b** is prevented from recombination only by the surrounding rigid matrix cage. Annealing of the matrix at temperatures above 25 K results in the rapid formation of bromo-2,2,2-trifluoro diphenylethane **13b**, which was identified by comparison of its IR spectrum with that of an authentic matrix-isolated sample (see SI).

DFT, MCSCF and DFT-D/MM Calculations. At the B97-D3/def2-TZVP level of theory, **6** is predicted to have a triplet ground state lying 6.1 kcal/mol below the lowest singlet state. The singlet carbene interacts strongly with CF_3I, and the calculated interaction energy of the resulting halogen bonded complex S-**10a** is −15.8 kcal/mol. In contrast, the interaction of the triplet carbene with CF_3I is much weaker, and the stabilization energy of T-**10a** is only −6.0 kcal/mol. Thus, the stabilization of the singlet carbene by halogen bonding is 9.8 kcal/mol larger than that of the triplet carbene, and this stabilization is larger than the singlet−triplet splitting of **6** of 6.1 kcal/mol. Consequently, the singlet state of the complex is lying 3.7 kcal/mol below the triplet state. This spin inversion is also found by QM/MM (B97-D3/def2-TZVP//CHARMM) calculations in explicit argon matrices. There, the S-T gap is inverted from 5.3 kcal/mol to −4.1 kcal/mol upon formation of the halogen bonded complexes (Figure 6). Similar changes in the S-T gap are also predicted by DFT calculations with other functionals; for example, from 6.8 to 0.4 kcal/mol with M06-2X/def2-TZVP and from 3.3 to −7.5 kcal/mol with BLYP-D3/def2-TZVP (Table S22, SI).

With CF_3Br, singlet carbene S-**6** forms a halogen-bonded complex with a stabilization energy of −10.7 kcal/mol (S-**10b**), while T-**6** forms a weaker complex with a stabilization energy of only −4.1 kcal/mol (T-**10b**). Again, the singlet complex S-**10b** is calculated to be more stable than the triplet complex T-**10b**, however, by only 0.5 kcal/mol (Figure S10, SI).

This behavior is analogous to the one observed for the interaction of **6** with methanol and water (see Table S8, SI for

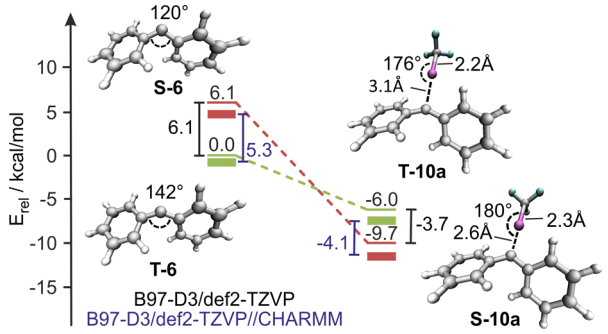

Figure 6. Relative energies and some geometric parameters of singlet and triplet **6** and the corresponding halogen bonded complexes with CF_3I T-**10a** and S-**10a** in the gas phase and in an explicit argon matrix, computed at the B97-D3/def2-TZVP and B97-D3/def2-TZVP//CHARMM levels of theory. All energies are in kcal/mol and corrected for ZPE, gas phase energies also for BSSE. The green and red bars represent the range of QM/MM values within several snapshots.

the interaction energies of DPC complexes with methanol, CF_3I and CF_3Br). When comparing the CH_3OH complexes of S- and T-**6** with the XCF_3 complexes, similar stabilization energies for the interactions with triplet T-**6** are predicted, suggesting that halogen bond (with iodine) and hydrogen bond to the triplet carbene show similar strengths. The situation is different for the interaction with S-**6**, where the halogen bond is about 5 kcal/mol stronger than the hydrogen bond. This can be rationalized by comparing the molecular orbitals involved in halogen and hydrogen bonding (Figure S11, SI). As expected, the main interaction between S-**6** and CF_3I is found between the HOMO of S-**6** (the nonbonding orbital at the carbene center) and the LUMO of CF_3I (the σ^* orbital). The corresponding interaction is also dominating the hydrogen bond in the S-**6**···$HOCH_3$ complex. For the halogen bond, back-donation from a lone pair at the iodine atom into the empty p orbital at the carbene center results in an additional stabilization of the halogen bond, which is lacking in the hydrogen bond. This type of interaction is not possible in T-**6**, where the p orbital at the carbene center contains an unpaired electron. This can also be illustrated using NBO theory (see SI).

When comparing the halogen bonding in **10a** with that in **10b**, the calculations predict a stronger interaction of the carbene with CF_3I than with CF_3Br. This is in line with the lower polarizability of the bromine atom compared to iodine, which generally results in weaker halogen bond complexes with bromine as donor than with iodine as donor. This can also be rationalized by the two orbital interactions discussed above. For the first type of interaction, the lower polarizability of bromine causes a smaller positive partial charge at Br in direction of the Br−C axis, leading to a weaker lone pair-σ^* interaction. In addition, since bromine is more electronegative than iodine, the back-donation will also be less favorable, leading to an overall weaker halogen bond with CF_3Br.

The computed gas-phase spectra of the type II complex **11a** nicely match the experimental results, although small imaginary modes indicate that the structure might not be a minimum in the gas phase. The computed dipole moments of 9.14 D for **10a** and 6.62 D for **11a** show that **11a** is of lower polarity than the classical halogen bond complex, suggesting that it is described better as a reversed halogen bond complex rather than an ion-pair.

DOI: 10.1021/jacs.5b12726
J. Am. Chem. Soc. XXXX, XXX, XXX−XXX

Although for the type II complex in the gas phase a minimum could not be definitively located, the QM/MM calculations reveal that in solid argon it is clearly a minimum. There, the type II structure is 0.5 kcal/mol higher in energy than the type I complex. Calculations of the reaction path for the interconversion of the singlet complexes **10a** and **11a** (B97-D3/def2-TZVP) reveal a transition state connecting both structures lying only 0.6 kcal/mol above the type I complex **10a** (Figure S12, SI). However, the potential energy surface in this region is very flat, and the calculations indicate nearly degenerate structures, in agreement with the experimental results.

Multiconfigurational SCF (MCSCF) approaches have been reported to produce reliable S-T energy gaps in various systems.[33−35] Therefore, we used MCSCF calculations to compute the S-T energy gap and to investigate the intersystem crossing in the reaction of **6** and CF_3I. CASSCF(8,8) MP2 (referred to as CASMP2) single point calculations were performed on the DFT-optimized geometries of S-**10a** and T-**10a**. The 6-31G* basis set was assigned to the C, H and F atoms and the LANL2DZ basis set was used for the iodine atom. As indicated above, the active space was formed by 8 electrons and 8 orbitals (Figure S13, SI, for more active space details see SI). Potential energy scans were performed for S-**10a** and T-**10a** along the C−I distance at the DFT level and single-point CASMP2 energies were calculated (Figure 7A). The S-T energy gap obtained from the CASMP2 calculations is −0.9 kcal/mol for **10a**, whereas the S-T energy gap of **6** was found to be 9.2 kcal/mol, at the same level of theory. These results support the inversion of the S-T energy gap obtained at the DFT level. The singlet and triplet potential energy surfaces were found to cross each other at the C−I distance of 3.25 Å. Additionally, we calculated CASMP2 energies for the Franck−Condon triplet state with the nuclear configuration of the singlet state (FC triplet). The corresponding curve crosses the singlet potential energy surface at 3.90 Å, indicating that the intersystem crossing may occur when the C−I distance is between 3.25 and 3.90 Å. Furthermore, the spin−orbit coupling between the singlet and triplet states calculated at this crossing point is 55.1 cm^{-1} (CASSCF(8,8) level of theory). This strong spin−orbit coupling (due to the presence of a heavy atom, I) may facilitate the intersystem crossing.

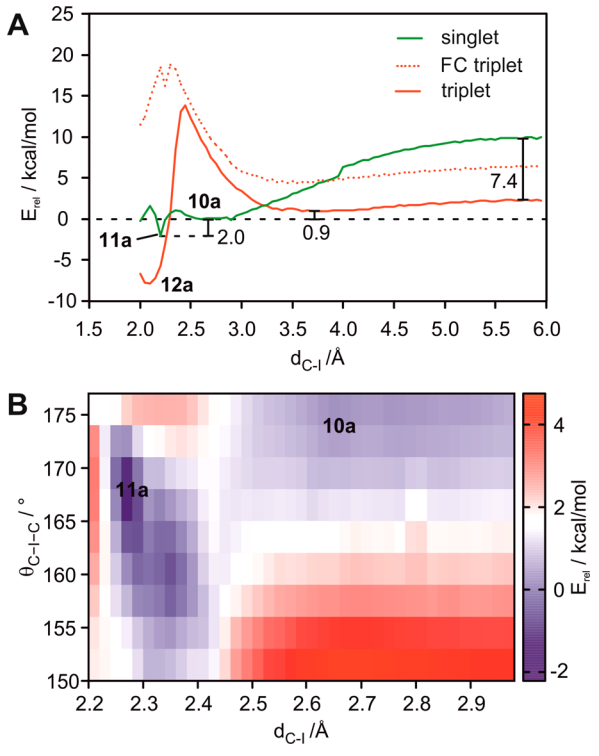

Figure 7. (A) Crossing point between singlet and triplet potential energy surfaces of **10a**. The potential energy surface was obtained by performing constrained optimizations along the C−I distance. The S-T energy gaps for **10a**, and locations of **11a** and **12a** are also indicated in the figure. (B) 2D-potential energy scan, using the halogen bonding distance and angle as reaction coordinates. The potential energy surfaces were constructed by single point CASMP2 calculations on the DFT-optimized geometries.

The CASMP2 calculations predict that **11a** is more stable than S-**10a** by 2.0 kcal/mol (Figure 7A). For a more precise estimation of this energy difference, we performed the potential energy scan with a finer reaction coordinate window (0.01 Å), between 2.1 and 2.8 Å. As shown in Figure S15, the two minima (S-**10a** and **11a**) were found to be equally stable, however with a barrier separation of 1 kcal/mol.

We also performed a 2-dimensional potential energy scan (with the halogen bond distance and angle as reaction coordinates) to explore the relative stability of S-**10a** and **11a**. Interestingly, **11a** (which is characterized by a C−I distance of 2.3 Å) exhibits stability over a range of C−I−C angles and S-**10a** (characterized by a nearly linear C−I−C angle) is stable over a range of C−I distances (d_{C-I}, Figure 7B). These calculations also corroborate that **11a** is slightly more stable than S-**10a**, and support the presence of a small barrier between these structures.

Additionally, we constructed a 2-dimensional potential energy surface at the CASMP2//DFT level, as a function of the distance d_{C-I} and the carbene angle (C−C−C). For this purpose, we performed series of geometry optimizations for a range of C−C−C angles between 120°−140° (resolution of 2°) and d_{C-I} distances between 2.5 and 4.0 Å (resolution of 0.02 Å). We found that the S-**10a** and T-**10a** potential energy surfaces cross each other along a "seam" (where S and T are degenerate),[36,37] which has a sloped topology (Figure 8). The reaction pathway outlined in Scheme 1 can be described as follows: triplet carbene T-**6** forms a relatively weak complex T-**10a** upon encountering CF_3I, which subsequently undergoes intersystem crossing to form S-**10a**. The minimum energy crossing point for this pathway is calculated to be at ∼4 kcal/mol (Figure 8, θ_{C-C-C} = 125°, d_{C-I} = 3.2 Å). Alternatively, T-**10a** may avoid crossing and form **12a** upon photoirradiation.

To explore if the type II complex **11a** is thermally accessible from S-**10a**, QM MD and QM/MM MD simulations were performed in the gas phase and in argon matrix. The singlet complexes **10a** and **11a** were used as starting structures, and the simulations were performed at temperatures of 3, 25, 50, and 75 K. In these simulations, all Ar atoms with a distance larger than 12 Å from the carbene center were kept frozen, effectively preventing the argon matrix to evaporate, even at elevated temperatures. In the simulations at 3, 25, and 50 K (both gas phase and argon matrix), the system remained in the initial conformation during the whole length of the simulations (10 ps), suggesting that at these temperatures thermal interconversion does not take place on a time scale of picoseconds. Interestingly, the simulation in the explicit argon matrix at 75 K exhibited a fast and reversible conversion of S-**10a** to **11a** (Figure 9).

DOI: 10.1021/jacs.5b12726
J. Am. Chem. Soc. XXXX, XXX, XXX−XXX

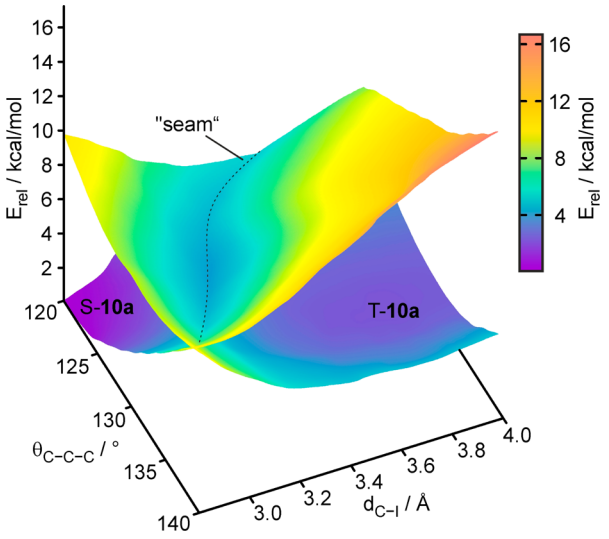

Figure 8. Potential energy scan for **10a** as a function of the carbene angle and the C···I distance showing the intersection seam between the singlet and triplet surface. The potential energy scan was performed by a series of single point CASSCF(8,8)MP2 calculations on the DFT-optimized geometries.

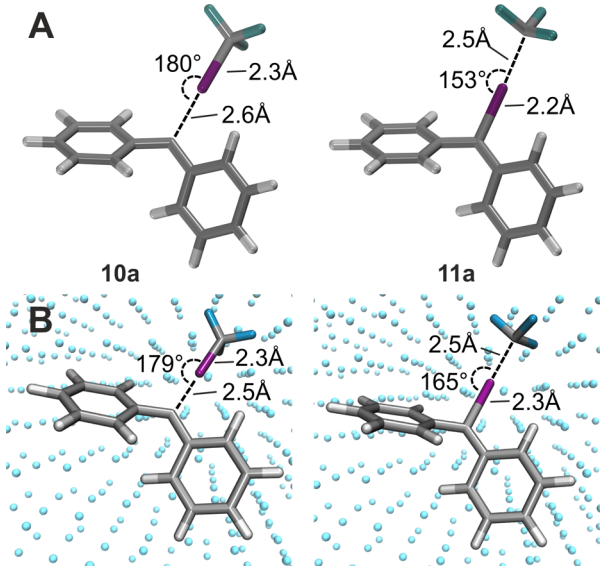

Figure 9. Snapshots from the QM MD and QM/MM MD simulations started from the type I complex (S-**10a**) at 75 K, indicate that both types of halogen bonded complexes are formed. (a) QM gas phase simulation at the B97-D3/def2-TZVP level (b) QM/MM simulation at the B97-D3/def2-TZVP//CHARMM level.

Additional QM MD simulations were performed at higher temperatures (100, 200, and 300 K). At these temperatures the gas phase simulations indicate a rapid interconversion between type I and type II complexes, resulting in both structures being populated independently of the starting geometry. Although these temperatures are unrealistic in the matrix, QM/MM MD simulations in argon were also performed at these temperatures. The interconversion between type I and type II complexes was also found under these conditions. This dynamic behavior is consistent with energetically nearly degenerate structures connected by a very small activation barrier, in agreement with the experiments.

CONCLUSION

Halogen bonding not only influences the thermodynamic stability and structure of stable molecular aggregates, but can also drastically change the properties of reactive intermediates such as carbenes. The results from IR, UV−vis, and EPR experiments in combination with calculations at various levels of theory allow us to draw a clear picture of how halogen bonding changes the properties of diphenylcarbene **6**:

(1) The closed shell singlet state of DPC (S-**6**) is an excellent halogen bond acceptor and forms very strong halogen bonds with both CF_3I and CF_3Br as halogen bond donors. However, since DPC has a triplet ground state (T-**6**), intersystem crossing is required concurrently with the formation of the halogen bond to form the singlet carbene complexes $Ph_2C\cdots X\text{-}CF_3$ **10a** and **11a**, respectively.

(2) With both CF_3I and CF_3Br the halogen-bonded singlet S-**6** becomes the ground state, which clearly demonstrates that with these donors the halogen bond stabilization of S-**6** compared to that of T-**6** is larger than the singlet−triplet gap of **6**. This is in agreement with DFT calculations which, as expected, predict for CF_3I a stronger halogen bond than for CF_3Br. For CF_3Br the singlet and triplet complexes are predicted to be almost degenerate.

(3) The IR and UV−vis spectra of the complexes $Ph_2C\cdots X\text{-}CF_3$ **10a** and **11a** clearly demonstrate that the singlet state S-**6** and not the triplet state T-**6** is involved in halogen bonding. A comparison with the hydrogen-bonded complexes[15,16] $Ph_2C\cdots H{-}OH$ and $Ph_2C\cdots H{-}OCH_3$ suggests that, despite the close similarity of the spectra of S-**6**, the interaction with $X\text{-}CF_3$ is stronger than that with H-OR. The stronger interaction results in a noticeable blue-shift and splitting into two components of the asymmetrical CCC stretching vibration involving the carbene center. This is in line with the calculated higher binding energies of the halogen-bonded complexes compared to the hydrogen-bonded complexes.

(4) The most striking difference between CF_3I and CF_3Br as halogen bond donors is that CF_3I leads to two energetically almost degenerate complexes **10a** and **11a** that easily interconvert, whereas CF_3Br forms only one complex **10b** with carbene S-**6**. We classify complexes **10a** and **11a** as conventional type I and nonconventional type II complex, respectively, as suggested by Donoso-Tauda et al. for a series of halogen-bonded NHC complexes.[13] According to these authors, type I complexes are formed if the R-X bond dissociation energy of the halogen bond donor is larger than 70 kcal/mol, whereas type II complexes are more likely if the BDE is below 60 kcal/mol. The BDE of CF_3I was determined to 52 kcal/mol,[38] which is below the 60 kcal/mol threshold. Since S-**6** is a stronger base[39,40] and a stronger halogen-bond acceptor than **3**, the abstraction of a halogen atom from R-X is thermodynamically even more favorable. Obviously, with 71 kcal/mol[41] the BDE of the C−Br bond in CF_3Br is too large for the formation of the type II complex **11b**.

Complexes **10a** and **11a** are in thermodynamic equilibrium even at the lowest matrix temperature, which implies an extremely low activation barrier for the interconversion. The experiments also indicate that

DOI: 10.1021/jacs.5b12726
J. Am. Chem. Soc. XXXX, XXX, XXX−XXX

photolysis of the matrix shifts the equilibrium toward complex **10a**. The nonclassical complex **11a** is slightly more stable according to the experiment. The DFT calculations predict **10a** to be more stable by approximately 0.5 kcal/mol, but this small difference is beyond the accuracy of these calculations. Furthermore, our multireference CASSCF(8,8) MP2 calculations correctly predict **11a** to be more stable than **10a** by 2 kcal/mol (Figure 7B).

The two complexes **10a** and **11a** differ mainly in the position of the iodine atom, and the rearrangement formally corresponds to a transfer of an I^+ ion, similar to a proton transfer in a hydrogen bonded system. In addition to ion transfer, halogen bonded systems can also undergo electron transfer to produce radicals, which adds another dimension of complexity to their chemistry.

(5) The thermal reaction of triplet DPC T-**6** with CF_3X to give the final C-X insertion products **13** is a highly complex reaction sequence involving three subsequent intersystem crossing steps. Thus, the triplet carbene T-**6** reacts to the singlet complex **10** (and in the case of CF_3I also to the second singlet complex **11a**) that forms the triplet radical pair **12**, which finally recombines to give the singlet insertion product **13** (Schemes 1 and 2). The CASSCF(8,8)MP2 calculations for the reaction with CF_3I provide detailed insight into these processes, and in particular rationalize the smooth formation of complex **10a**.

(6) Interestingly, our experiments do not give any evidence for the formation of an ylide or ylidic complex[42] with CF_3X acting as Lewis base and the carbene S-**6** with its vacant p orbital acting as Lewis acid. Ylides formed between singlet carbenes and ethers,[43,44] alcohols,[45] pyridine,[46,47] and other reagents bearing lone pairs are frequently observed as intermediates. Obviously, halogen bonding is energetically favored over ylide formation in the reactions investigated here. It remains an interesting challenge for future research to find carbenes where ylide formation is preferred over halogen bonding.

In summary, halogen bonding to reactive carbenes is an effective tool to control the spin state and the reactivity of carbenes. The work presented here suggests that halogen bonding has to be considered as an important mechanism for the stabilization of reactive carbenes that might rival the long discussed formation of ylidic complexes, and that can surpass the stability of hydrogen-bonded complexes.

EXPERIMENTAL SECTION

General Procedures. Preparation of diphenyldiazomethane **9** and matrix isolation measurements were carried out according to procedures described in preceding work.[15,16] Matrices were doped with ICF_3 (Fluorochem) and $BrCF_3$ (Aldrich Chemical Co.) as commercially available.

Computational Details. All gas phase geometry optimizations and frequency calculations were performed using the B97[48] functional with D3 dispersion corrections[49] as implemented in the program Turbomole (version 6.4).[50] The def2-TZVP[51] basis set was used. NBO analysis was performed using the NBO version 6 program.[52]

QM MD, QM/MM MD simulations and QM/MM optimizations were performed using the program ChemShell[53,54] as interface to Turbomole for the QM region (DPC and CF_3I) and CHARMM 31b1[55] for the MM region (argon matrix). QM MD simulations were conducted at the B97-D3/def2-SVP level of theory while QM/MM MD simulations were carried out at the B97-D3/def2-SVP//CHARMM level. In both cases, 10 ps MD simulations were performed with a time step of 2 fs under NVT (canonical) conditions at temperatures of 3, 25, 50, 75, 100, 200, and 300 K. A Nosé−Hoover chain thermostat[56,57] was used together with a reversible noniterative leapfrog-type integrator. In the setup for the MD simulations, the gas phase optimized structures of the DPC - CF_3I complexes were used as starting geometry for the QM region, which was then placed in a pre-equilibrated box of argon with 15 Å padding. The surrounding MM atoms were equilibrated for 5 ns under NPT conditions in the presence of a frozen QM region. Afterward, production QM/MM MDs simulations were performed in which the QM region and all MM atoms within 10 Å of the QM region were allowed to freely move. Ten snapshots were taken from each of the QM/MM MD simulations and reoptimized at the B97-D3/def2-TZVP//CHARMM level of theory. All atoms within the active region were allowed to move in each optimization step. The optimization was finished when the maximum gradient component was below 0.00045 au

The GAUSSIAN09 suite of programs was used for the CASSCF and CASMP2 calculations.[58,59] The structures of S-**10a** and T-**10a** were optimized at the B97-D3/def2-TZVP level. The potential energy scan was performed along the carbene center-I distance (d_{C-I}), in the range from 2 to 6 Å with the step size of 0.05 Å. At each point, the positions of C and I were fixed, and the rest of the structure was optimized. These DFT optimized geometries were used for CASSCF and CASMP2 single point calculations (see SI). For all the CAS calculations, the 6-31G* basis set was used for C, H and F atoms and the LANL2DZ basis set and Effective Core Potential (ECP) were used for the I atom.[60] Only ground state CAS calculations were performed. The configurations having CI coefficients larger than 0.1 were used as reference states for Møller−Plesset perturbation theory (MP2) level electron correlation.[61,62] Spin−orbit coupling was calculated at the intersection of the singlet and triplet potential energy surfaces.[63,64]

ASSOCIATED CONTENT

Supporting Information

The Supporting Information is available free of charge on the ACS Publications website at DOI: 10.1021/jacs.5b12726.

Spectroscopic and computational data. (PDF)

AUTHOR INFORMATION

Corresponding Authors

*esanchez@kofo.mpg.de

*wolfram.sander@rub.de

Notes

The authors declare no competing financial interest.

ACKNOWLEDGMENTS

This work was supported by the Cluster of Excellence RESOLV (EXC 1069) funded by the Deutsche Forschungsgemeinschaft (DFG). P.S. and E.S.-G thank Rachel Crespo-Otero for useful discussions. E.S.-G acknowledges the support from the Boehringer Ingelheim Foundation (Plus-3 Program) and a Liebig-stipend from the Fonds der Chemischen Industrie, as well as the support of the Collaborative Research Center SFB1093, funded by the DFG. We thank Nesli Özkan for performing some of the CF_3Br experiments and Stefan Huber for introducing us to halogen bonded systems.

REFERENCES

(1) Wolters, L. P.; Bickelhaupt, F. M. *ChemistryOpen* **2012**, *1*, 96.
(2) Tawfik, M.; Donald, K. J. *J. Phys. Chem. A* **2014**, *118*, 10090.
(3) Desiraju, G. R.; Ho, P. S.; Kloo, L.; Legon, A. C.; Marquardt, R.; Metrangolo, P.; Politzer, P.; Resnati, G.; Rissanen, K. *Pure Appl. Chem.* **2013**, *85*, 1711.

DOI: 10.1021/jacs.5b12726
J. Am. Chem. Soc. XXXX, XXX, XXX−XXX

(4) Huber, S. M.; Scanlon, J. D.; Jimenez-Izal, E.; Ugalde, J. M.; Infante, I. *Phys. Chem. Chem. Phys.* **2013**, *15*, 10350.
(5) Priimagi, A.; Cavallo, G.; Metrangolo, P.; Resnati, G. *Acc. Chem. Res.* **2013**, *46*, 2686.
(6) Robertson, C. C.; Perutz, R. N.; Brammer, L.; Hunter, C. A. *Chem. Sci.* **2014**, *5*, 4179.
(7) Meyer, F.; Dubois, P. *CrystEngComm* **2013**, *15*, 3058.
(8) Jungbauer, S. H.; Bulfield, D.; Kniep, F.; Lehmann, C. W.; Herdtweck, E.; Huber, S. M. *J. Am. Chem. Soc.* **2014**, *136*, 16740.
(9) Walter, S. M.; Kniep, F.; Herdtweck, E.; Huber, S. M. *Angew. Chem., Int. Ed.* **2011**, *50*, 7187.
(10) Kniep, F.; Jungbauer, S. H.; Zhang, Q.; Walter, S. M.; Schindler, S.; Schnapperelle, I.; Herdtweck, E.; Huber, S. M. *Angew. Chem., Int. Ed.* **2013**, *52*, 7028.
(11) Arduengo, A. J., III; Kline, M.; Calabrese, J. C.; Davidson, F. *J. Am. Chem. Soc.* **1991**, *113*, 9704.
(12) Arduengo, A. J., III; Tamm, M.; Calabrese, J. C. *J. Am. Chem. Soc.* **1994**, *116*, 3625.
(13) Donoso-Tauda, O.; Jaque, P.; Elguero, J.; Alkorta, I. *J. Phys. Chem. A* **2014**, *118*, 9552.
(14) Lv, H.; Zhuo, H.-Y.; Li, Q.-Z.; Yang, X.; Li, W.-Z.; Cheng, J.-B. *Mol. Phys.* **2014**, *112*, 3024.
(15) Costa, P.; Sander, W. *Angew. Chem., Int. Ed.* **2014**, *53*, 5122.
(16) Costa, P.; Fernandez-Oliva, M.; Sanchez-Garcia, E.; Sander, W. *J. Am. Chem. Soc.* **2014**, *136*, 15625.
(17) Costa, P.; Trosien, I.; Fernandez-Oliva, M.; Sanchez-Garcia, E.; Sander, W. *Angew. Chem., Int. Ed.* **2015**, *54*, 2656.
(18) Eisenthal, K. B.; Turro, N. J.; Sitzmann, E. V.; Gould, I. R.; Hefferon, G.; Langan, J.; Cha, Y. *Tetrahedron* **1985**, *41*, 1543.
(19) Eisenthal, K. B.; Moss, R. A.; Turro, N. J. *Science* **1984**, *225*, 1439.
(20) Griller, D.; Nazran, A. S.; Scaiano, J. C. *J. Am. Chem. Soc.* **1984**, *106*, 198.
(21) Wright, B. B.; Platz, M. S. *J. Am. Chem. Soc.* **1984**, *106*, 4175.
(22) Leyva, E.; Barcus, R. L.; Platz, M. S. *J. Am. Chem. Soc.* **1986**, *108*, 7786.
(23) Herrebout, W. *Top. Curr. Chem.* **2014**, *358*, 79.
(24) Nagels, N.; Herrebout, W. A. *Spectrochim. Acta, Part A* **2015**, *136*, 16.
(25) Hauchecorne, D.; Herrebout, W. A. *J. Phys. Chem. A* **2013**, *117*, 11548.
(26) Romaniello, P.; Lelj, F. *J. Phys. Chem. A* **2002**, *106*, 9114.
(27) Ito, F.; Hirabayashi, S. *J. Chem. Phys.* **2006**, *124*, 234509-1.
(28) Sander, W. W. *J. Org. Chem.* **1989**, *54*, 333.
(29) Clemitshaw, K. C.; Sodeau, J. R. *J. Phys. Chem.* **1988**, *92*, 5491.
(30) Forney, D.; Jacox, M. E.; Irikura, K. K. *J. Chem. Phys.* **1994**, *101*, 8290.
(31) Gibbons, W. A.; Trozzolo, A. M. *J. Am. Chem. Soc.* **1966**, *88*, 172.
(32) Edlund, O.; Lund, A.; Shiotani, M.; Sohma, J.; Thuomas, K. A. *Mol. Phys.* **1976**, *32*, 49.
(33) Cui, G.; Fang, W. *J. Chem. Phys.* **2013**, *138*, 044315.
(34) Mai, S.; Marquetan, P.; González, L. *J. Phys. Chem. A* **2015**, *119*, 9524.
(35) Uzunova, E. L. *J. Phys. Chem. A* **2009**, *113*, 11266.
(36) Paterson, M. J.; Robb, M. A.; Blancafort, L.; DeBellis, A. D. *J. Phys. Chem. A* **2005**, *109*, 7527.
(37) Bernardi, F.; Olivucci, M.; Robb, M. A. *Chem. Soc. Rev.* **1996**, *25*, 321.
(38) Okafo, E. N.; Whittle, E. *Int. J. Chem. Kinet.* **1975**, *7*, 273.
(39) Keeffe, J. R.; O'Ferrall, R. A. M. *ARKIVOC (Gainesville, FL, U. S.)* **2008**, 183.
(40) Pliego, J. R.; DeAlmeida, W. B. *J. Chem. Soc., Faraday Trans.* **1997**, *93*, 1881.
(41) Ferguson, K. C.; Whittle, E. *J. Chem. Soc., Faraday Trans. 1* **1972**, *68*, 295.
(42) Moss, R. A. *J. Phys. Org. Chem.* **2011**, *24*, 866.
(43) Moss, R. A.; Wang, L.; Odorisio, C. M.; Zhang, M.; Krogh-Jespersen, K. *J. Phys. Chem. A* **2010**, *114*, 209.
(44) Hoijemberg, P. A.; Moss, R. A.; Krogh-Jespersen, K. *J. Phys. Chem. A* **2012**, *116*, 358.
(45) Xue, J.; Luk, H. L.; Platz, M. S. *J. Am. Chem. Soc.* **2011**, *133*, 1763.
(46) Jones, M. B.; Platz, M. S. *J. Org. Chem.* **1991**, *56*, 1694.
(47) Admasu, A.; Gudmundsdottir, A. D.; Platz, M. S. *J. Phys. Chem. A* **1997**, *101*, 3832.
(48) Grimme, S. *J. Comput. Chem.* **2006**, *27*, 1787.
(49) Grimme, S.; Antony, J.; Ehrlich, S.; Krieg, H. *J. Chem. Phys.* **2010**, *132*, 154104.
(50) *TURBOMOLE* V6.4 2012; TURBOMOLE GmbH, 2007; www.turbomole.com.
(51) Weigend, F.; Häser, M.; Patzelt, H.; Ahlrichs, R. *Chem. Phys. Lett.* **1998**, *294*, 143.
(52) *NBO 6.0*; Glendening, E. D.; Badenhoop, J. K.; Reed, A. E.; Carpenter, J. E.; Bohmann, J. A.; Morales, C. M.; Landis, C. R.; Weinhold, F.; Theoretical Chemistry Institute, University of Wisconsin: Madison, WI, 2013.
(53) *ChemShell, a Computational Chemistry Shell*; www.chemshell.org.
(54) Metz, S.; Kästner, J.; Sokol, A.; Keal, T. W.; Sherwood, P. *Wiley Interdiscip. Rev. Comput. Mol. Sci.* **2014**, *4*, 101.
(55) Brooks, B. R.; Brooks, C. L.; Mackerell, A. D.; Nilsson, L.; Petrella, R. J.; Roux, B.; Won, Y.; Archontis, G.; Bartels, C.; Boresch, S.; Caflisch, A.; Caves, L.; Cui, Q.; Dinner, A. R.; Feig, M.; Fischer, S.; Gao, J.; Hodoscek, M.; Im, W.; Kuczera, K.; Lazaridis, T.; Ma, J.; Ovchinnikov, V.; Paci, E.; Pastor, R. W.; Post, C. B.; Pu, J. Z.; Schaefer, M.; Tidor, B.; Venable, R. M.; Woodcock, H. L.; Wu, X.; Yang, W.; York, D. M.; Karplus, M. *J. Comput. Chem.* **2009**, *30*, 1545.
(56) Nosé, S. *J. Chem. Phys.* **1984**, *81*, 511.
(57) Hoover, W. *Phys. Rev. A: At., Mol., Opt. Phys.* **1985**, *31*, 1695.
(58) Frisch, M. J.; Trucks, G. W.; Schlegel, H. B.; Scuseria, G. E.; Robb, M. A.; Cheeseman, J. R.; Scalmani, G.; Barone, V.; Mennucci, B.; Petersson, G. A.; Nakatsuji, H.; Caricato, M.; Li, X.; Hratchian, H. P.; Izmaylov, A. F.; Bloino, J.; Zheng, G.; Sonnenberg, J. L.; Hada, M.; Ehara, M.; Toyota, K.; Fukuda, R.; Hasegawa, J.; Ishida, M.; Nakajima, T.; Honda, Y.; Kitao, O.; Nakai, H.; Vreven, T.; Montgomery, J. A.; Peralta, J. E.; Ogliaro, F.; Bearpark, M.; Heyd, J. J.; Brothers, E.; Kudin, K. N.; Staroverov, V. N.; Kobayashi, R.; Normand, J.; Raghavachari, K.; Rendell, A.; Burant, J. C.; Iyengar, S. S.; Tomasi, J.; Cossi, M.; Rega, N.; Millam, J. M.; Klene, M.; Knox, J. E.; Cross, J. B.; Bakken, V.; Adamo, C.; Jaramillo, J.; Gomperts, R.; Stratmann, R. E.; Yazyev, O.; Austin, A. J.; Cammi, R.; Pomelli, C.; Ochterski, J. W.; Martin, R. L.; Morokuma, K.; Zakrzewski, V. G.; Voth, G. A.; Salvador, P.; Dannenberg, J. J.; Dapprich, S.; Daniels, A. D.; Farkas, Ö.; Foresman, J. B.; Ortiz, J. V.; Cioslowski, J.; Fox, D. J. *Gaussian 09*, Revision D.01; Gaussian Inc.: Wallingford, CT, 2009.
(59) Yamamoto, N.; Vreven, T.; Robb, M. A.; Frisch, M. J.; Schlegel, H. B. *Chem. Phys. Lett.* **1996**, *250*, 373.
(60) Hay, P. J.; Wadt, W. R. *J. Chem. Phys.* **1985**, *82*, 299.
(61) Head-Gordon, M.; Pople, J. A.; Frisch, M. J. *Chem. Phys. Lett.* **1988**, *153*, 503.
(62) McDouall, J. J. W.; Peasley, K.; Robb, M. A. *Chem. Phys. Lett.* **1988**, *148*, 183.
(63) Abegg, P. W. *Mol. Phys.* **1975**, *30*, 579.
(64) Marian, C. M. *Wiley Interdiscip. Rev. Comput. Mol. Sci.* **2012**, *2*, 187.

DOI: 10.1021/jacs.5b12726
J. Am. Chem. Soc. XXXX, XXX, XXX−XXX